Supplement of Ocean Sci., 22, 1587–1607, 2026
https://doi.org/10.5194/os-22-1587-2026-supplement

Ocean Science Open Access EGU

Supplement of

Analytical approaches for wave energy dissipation induced by wave-generated turbulence and random wave-breaking

Yongzeng Yang et al.

Correspondence to: Meng Sun (sunm@fio.org.cn)

Though the wave steepness in Table 1 in our manuscript is less than the classical breaking criterion 1/7, the breaking effects require further arguments. In the following, we explored the comprehensive tank experiments of Wei et al. (2018) concerning the surface drag coefficient, have expanded our analysis to provide more quantitative details on the effects of wave breaking, wind-driven turbulence, and Langmuir turbulence. The discrepancy between the model results and observations in Fig. 4 in our manuscript reveals that turbulence generation may be governed by complex dynamical mechanisms. Though the above dynamical processes are all important in the tank experiments, the shear instability of wave orbital motions appears to be the dominant contributor to turbulence.

S1.1 Effects of wave breaking

In the paper of Wei et al. (2018), the effects of wave breaking were not addressed. A separate series of laboratory experiments on the measurement of the surface drag coefficient touched upon this issue (Wei, 2017). Figure (Fig. 3-4 of Wei, 2017) shows that the surface drag coefficient increase with wind speed when wind speed at 15-30 m s^{-1}. When the wind speed is larger than 30 m s^{-1}, the surface drag coefficient shows a marked drop. He further added to the wave tank a modest amount of foam (produced by mixing dish soap and water) and half of the foam, in order to study the influence of surface foam on the drag coefficient. Comparisons among the three scenarios: not adding foam, adding half the foam and adding full foam show finer details (Fig. 3-7 of Wei, 2017). Foam increases surface drag coefficient at low wind speed. With wind speed increases, it decreases surface drag coefficient. The drag coefficient does not change significantly when the wind speed exceeds 30 m s^{-1}, which is mainly due to the breaking foam of surface waves (Wei, 2017). His series of laboratory measurements show that breaking effects are negligible, except when wind speeds exceed 30 m s^{-1}. For the final scenario, i.e., Experiment 2 in Table 1 in our manuscript, precisely quantifying the effect of breaking is difficult, and his experimental setup was not specifically designed to address this issue. Lamarre and Melville (1991) measured the breaking entrainment depth and derived the result of $0.015\overline{L}$-$0.05\overline{L}$, and the measurements of Kalvoda et al. (2003) satisfy the results of $0.2H_s$-$0.5H_s$. The latest experimental study found that the penetration depth of breaking-wave-generated turbulence is $0.7H_s$-$0.9H_s$ (Mu et al., 2021), which is consistent with the findings of Rapp and Melville (1990) and Hwang et al. (2016). So the maximum wave-breaking penetration depth is approximately 5 cm for Experiment 2, which is about one-quarter to one-third of the observed ε_{dis} depth, and the latter can reach a depth of 15-20 cm (see Fig. 4 in our manuscript). So the breaking events in Experiment 2 appear to be micro-breaking, rather than full wave breaking. This does not imply that micro-breaking is absent in Experiment 1, and in realistic sea states, wave breaking is perpetually present and, as such, constitutes an essential

dissipation source term in the modern widely-applied third-generation wave models. Wei et al. (2018) may not have specifically addressed the effects of micro-breaking, which we will evaluate in the discussion below.

S1.2 Estimates of the wave breaking, wind-driven TKE dissipation rate

In the following, we attempt to employ the parameterization approach of Wang and Liao (2016) to derive somewhat quantitative estimates of the wind-driven near surface TKE dissipation rate and compare them with our results for the wind-wave Experiments 1-2 (see Table 1 in our manuscript). The measured turbulence in the top layer on Lake Michigan (without noticeable wave breakers, i.e., whitecaps) is likely due to the TKE production through wind shear, micro-breaking events of surface waves by comparing with the Law-Of-the-Wall (LOW) scaling (Wang and Liao, 2016). Based on the arguments of the additional TKE flux from the wave breaking to the wind shear (Terray et al.,1996; Sutherland and Melville, 2015), they proposed an improved parameterization to include wave age in the scaling to account for its impact on the near surface turbulent dissipation rate, i.e.,

$$\varepsilon_{\text{win}} = \begin{cases} 1.3\times10^{-3}\dfrac{c_{\text{p}}A_{\text{g}}u_{*\text{w}}^2}{H_{\text{s}}}\left(\dfrac{x_3}{H_{\text{s}}}\right)^{-0.7} & \text{if } \dfrac{x_3}{H_{\text{s}}} < 0.4 \\ 1.4\times10^{-3}\dfrac{c_{\text{p}}A_{\text{g}}u_{*\text{w}}^2}{H_{\text{s}}}\left(\dfrac{x_3}{H_{\text{s}}}\right)^{-2} & \text{if } \dfrac{x_3}{H_{\text{s}}} \geq 0.4 \end{cases} \quad \text{(S1)}$$

where H_{s} is the significant wave height, c_{p} is the characteristic wave phase speed, $u_{*\text{w}}$ is the water-side friction velocity, and A_{g} is the wave age defined as the ratio of the characteristic wave phase speed to the friction velocity at air side, i.e., $A_{\text{g}} \equiv c_{\text{p}}/u_{*\text{a}}$. Profiles of normalized dissipation rate were also compared with previous literature observations.

In the numerical estimation below, only the second fraction in Eq. (S1) is employed for the tank observation points of Wei et al. (2018) meet only the second condition, i.e., $x_3/H_{\text{s}} > 0.4$. Two parameters H_{s} and c_{p} can be derived directly from Table 1 in our manuscript, where the wave dispersion relation is applied. The air-side $u_{*\text{a}}$ is calculated from the measured drag coefficient from Wei (2017), i.e., $u_{*\text{a}} = \sqrt{C_{\text{d}}}\cdot U_{10}$ and the water-side friction velocity $u_{*\text{w}}$ is calculated by using $u_{*\text{w}} = \sqrt{\dfrac{\rho_{\text{a}}}{\rho_w}}\cdot u_{*\text{a}}$, where ρ_{a}, ρ_w represent the air density and water density, respectively. Figure S1 shows the dependence of TKE dissipation rate of wind-driven turbulence (dashed lines) versus layer depth in linear/logarithmic scale for wind wave conditions respectively. The estimated TKE dissipation rates varies in the range of 10^{-7}-10^{-4} m^2 s^{-3}, which are 1-2 orders of magnitude smaller than the laboratory observations of Wei et al. (2018). We also note that, though the 10m wind speed U_{10} in the wind wave Experiments 1-2 is much higher than that (2.7-14.3 m s^{-1}) over the Lake Michigan, the estimated TKE dissipation rates of wind-driven turbulence at a water depth of 10 cm are smaller than

the observations over the lake. This is mainly due to the short wave age (0.77 and 0.57) in the wind wave Experiments 1-2 (the wind wave tank is only 16 m long with a short fetch), which is much smaller than that (2.7 - 52.6) over the lake. In this context, the influence of turbulence generated by wind shear and micro-breaking events in the wind wave Experiments 1-2 can be considered negligible. And for the mixed wave Experiment 3, the influence of the wind-driven turbulence component can also be considered negligible.

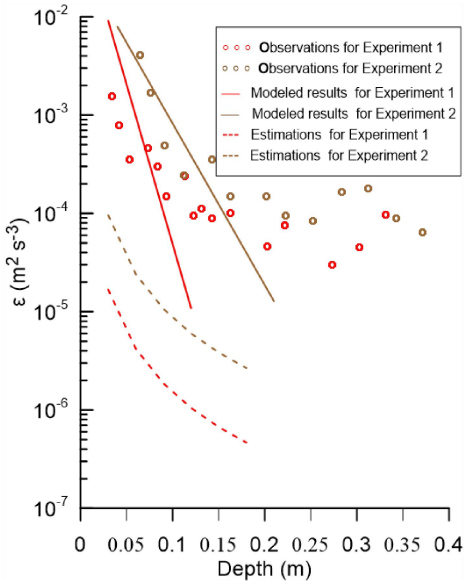

Figure S1. Dependence of TKE dissipation rate $\varepsilon_{\mathrm{dis}}$ (denoted as ε in the figure) versus layer depth. Observation data for wind waves (circles) are digitalized from Wei et al. (2018). The estimations of the TKE dissipation rate of wave-generated turbulence (Eq. (19) in our manuscript) and wind-driven turbulence (Eq. (S1)) are shown with solid and dashed lines, respectively. Data are plotted in linear/logarithmic scale on the horizontal/vertical axis.

S1.3 Estimates of the TKE dissipation rate of Langmuir turbulence

Polton and Belcher (2007), Grant and Belcher (2009) present a highly valuable characteristics scaling of Langmuir turbulence by using the large-eddy simulation (LES) scheme. When the Stokes drift of the wave field is sufficiently large compared to the surface friction velocity, their scaling leads to unique profiles of nondimensional dissipation rate. And the shapes of the LES dissipation profiles agree well with the observations, the Langmuir numbers for these profiles are in the range of 0.15-0.30 (Grant and Belcher, 2009). Based on the measured drag coefficient and the calculated water-side friction velocity $u_{*\mathrm{w}}$ stated above, as well as the Stokes drift $U_{\mathrm{S}} = \omega K A^2 \exp\{2Kx_3\}$ (Mcwilliams et al., 1997), we calculate the corresponding turbulent Langmuir numbers for Experiments 1-3 (see Table S1 below). In the following, we attempt to estimate the TKE dissipation rate resulting solely from the Stokes drift

shear, including that for the swell Experiment 4. This leads us to adopt the turbulent k - ε model (Yuan et al., 2013) and its equilibrium solutions to estimate, which is also discussed in Appendix B in our manuscript where the shear term $\frac{\partial u_{\mathrm{SM}i}}{\partial x_j}$ (it consists of all the relevant shear terms induced by wave motion) is replaced by $\frac{\partial U_{\mathrm{S}}}{\partial x_3}$ i.e.,

$$\overline{k} \approx \pi \overline{l}_{\mathrm{D}}^{2} \left(\left| \frac{\partial U_{\mathrm{S}}}{\partial x_3} \right| \right)^2 \tag{S2}$$

$$\overline{\varepsilon} \approx \overline{l}_{\mathrm{D}}^{2} \left(\left| \frac{\partial U_{\mathrm{S}}}{\partial x_3} \right| \right)^3 \tag{S3}$$

So the Reynolds average of Eq. (S3) on wave motion is

$$\left\langle \overline{\varepsilon} \right\rangle_{\mathrm{SM}} \approx \left\langle \overline{l}_{\mathrm{D}}^{2} \right\rangle_{\mathrm{SM}} \left\langle \left(\left| \frac{\partial U_{\mathrm{S}}}{\partial x_3} \right| \right)^3 \right\rangle_{\mathrm{SM}} = \frac{1}{2} A^2 \exp\{2Kx_3\} \cdot \left\{ 2\omega K^2 A^2 \exp\{2Kx_3\} \right\}^3 = 4\omega^3 K^6 A^8 \exp\{8Kx_3\} \tag{S4}$$

Here we assume the relations $\overline{l}_{\mathrm{D}} \approx \left| A \exp\{Kx_3\} \exp\left\{ i \left(\boldsymbol{k} \cdot \boldsymbol{r} - \omega t \right) \right\} \right|$ and $\left\langle \overline{l}_{\mathrm{D}}^{2} \right\rangle_{\mathrm{SM}} \approx \frac{1}{2} A^2 \exp\{2Kx_3\}$ between the turbulent mixing length and the wave amplitude A. This reflects the effective scale of turbulent eddy motion and mixing in a wave-influenced environment. While this is a simplification, we deem it is a reasonable assumption for the scope of this study. In the following Fig. S2, the estimated TKE dissipation rates for Experiments 1-3 and the swell Experiment 4 in Table 1 are also shown. Comparison with Fig. 4 in our manuscript indicates the TKE dissipation rates of Langmuir turbulence are 1-2 orders of magnitude smaller than those from our model, and the estimated TKE dissipation rates are less than 10^{-6} $\mathrm{m^2\ s^{-3}}$ for the swell case. Though the turbulent Langmuir number $L_{\mathrm{a}} > 0.5$ for Experiments 1-3, the magnitude of the TKE dissipation rate resulting solely from the Stokes drift shear is comparable to that of the wind-driven turbulence displayed above.

Literature on this topic is considerable, e.g., a two equation (k - ε) model coupled to momentum equations, in which the Stokes-vortex forcing term was taken into account, were used to investigate the enhanced turbulence (Araujo et al., 2001). Skyllingstad (2005) analyzed the LES modeled TKE budget to clarify the entrainment affected by Langmuir circulation, including mean flow and Stokes shift shear-productions, vertical transport by turbulent eddies, Stokes-vortex forcing, etc. It must be acknowledged that our estimation method used here is a rather rough one and has some drawbacks e.g., only the Stokes shift shear-production is included, but the Coriolis-Stokes forcing, the Stokes-vortex forcing and convection/diffusion terms are not considered for the measurements of the flow field were not prioritized in the wave tank experiments. Polton and Belcher (2007) concluded that the conjunctive effects of the Coriolis-Stokes forcing and the Stokes-vortex forcing result in a reduced mean shear and enhanced vertical transport of TKE into the mixed layer. Our estimate above may be somewhat overestimated, which requires further study.

Table S1. Wave parameters and turbulent Langmuir numbers for selected wave conditions from Wei et al. (2018).

Experiment number	Wave condition	Significant wave height *Hs* (cm)	Peak frequency (Hz)	Wave length (m)	Turbulent Langmuir number L_a
1	21 m s^{-1} wind	3.75	2.72	0.42	0.60
2	32 m s^{-1} wind	6.03	1.97	0.83	0.84
3	1.6 Hz swell with 21 m s^{-1} wind	5.26	1.64	0.86	0.79
4	1.2 Hz swell	3.98	1.20	1.36	---

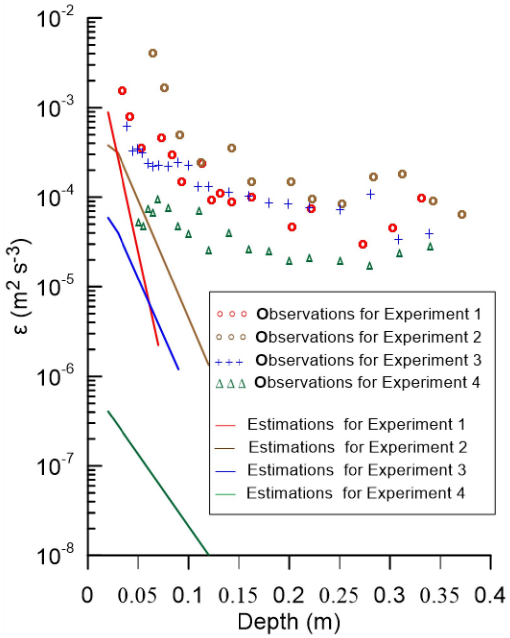

Figure S2. Dependence of TKE dissipation rate ε_{dis} (denoted as ε in the figure) versus layer depth. Observation data (circles, pluses and triangles) are digitalized from Wei et al. (2018). The estimations of the TKE dissipation rate of Langmuir turbulence are shown with solid lines. Data are plotted in linear/logarithmic scale on the horizontal/vertical axis.

References

Araujo, M., Dartus, D., Maurel, P., and Masbernat, L.: Langmuir circulations and enhanced turbulence beneath wind-waves, Ocean Modeling, 3, 109-126, 2001.

Grant, A. L. M., and Belcher, S. E.: Characteristics of Langmuir turbulence in the ocean mixed layer, J. Phys. Oceanogr., 39, 1871-1887, doi: 10.1175/2009JPO4119.1, 2009.

Kalvoda, P. M., Xu, L. L., Wu, J.: Macrobubble clouds produced by breaking wind waves: A laboratory study, J. Geophys. Res., 108, 3207, 2003.

Lamarre, E., and Melville, W. K.: Air entrainment and dissipation in breaking waves, Nature, 351, 469-472, 1991.

McWilliams, J. C., Sullivan P. P., and Moeng C.-H.: Langmuir turbulence in the ocean. J. Fluid Mech., 334, 1-30, 1997.

Mu, H., Liu, Y., Yuan, Y., Ju, L., Liu, J., Meng, J, and Chen, X.: Turbulent mixing during wave breaking: an experimental study, Oceanol. Limnol. Sin., 52(3), 551-561, 2021.

Polton, J. A., and Belcher, S. E.: Langmuir turbulence and deeply penetrating jets in an unstratified mixed layer, J. Geophys. Res., 112, C09020, doi:10.1029/2007JC004205, 2007.

Rapp, R. J., and Melville, W. K.: Laboratory measurements of deep-water breaking waves, Philosophical Transactions of the Royal Society of London A: Mathematical and Physical Sciences, 331(1622), 735-800, 1990..

Skyllingstad, E.: Langmuir circulation, in: Marine turbulence: theories, observations, and models, edited by: Baumert, H. Z., Simpson, J. H., and Sündermann, J., Cambridge University Press, Cambridge, UK, 630pp., ISBN 978-0-521-15372-0, 2005.

Sutherland, P., and Melville, W. K.: Field measurements of surface and near-surface turbulence in the presence of breaking waves, J. Phys. Oceanogr., 45(4), 943–965, https://doi.org/10.1175/JPO-D-14-0133.1, 2015.

Terray, E. A., Donelan, M., Agrawal, A. Y. C., Drennan,W. M., Kahma,K. K., Williams, A. J., Hwang, P. A., and Kitaigorodskii, S. A.: Estimates of kinetic energy dissipation under breaking waves, J. Phys. Oceanogr., 26(5), 792-807, 1996.

Wang, B., and Liao, Q.: Field observations of turbulent dissipation rate profiles immediately below the air-water interface, J. Geophys. Res. Oceans, 121, 4377-4391, https://doi.org/10.1002/2015JC011512, 2016.

Wei, L.: Laboratory research on air-sea interface boundary layer, Doctoral dissertation, Ocean University of China, Qingdao, 2017 (in Chinese).

Wei, L., Guan, C., and Troitskaya, Y.: Laboratory experiment on wave induced turbulence, J. Ocean Univ. China, 17 (4), 721-726,

https://doi.org/10.1007/s11802-018-3528-4, 2018.

Yuan, Y., Qiao, F., Yin, X., and Han, L.: Analytical estimation of mixing coefficient induced by surface wave-generated turbulence based on the equilibrium solution of the second-order turbulence closure model, Sci. China Earth Sci., 56, 71-80, https://doi.org/10.1007/s11430-012-4517-x , 2013.